MALAYSIAN JOURNAL OF ANALYTICAL SCIENCES

Journal homepage: https://mjas.analis.com.my/

Research Article

Optimized synthesis of Cu^{2+}-modified *Samanea saman*-derived carbon adsorbent for metformin adsorption

Mohd Raziff Mat Hasan, Erniza Mohd Johan Jaya, and Mohd Azmier Ahmad*

School of Chemical Engineering, Engineering Campus, Universiti Sains Malaysia, 14300 Nibong Tebal, Penang, Malaysia

*Corresponding author: chazmier@usm.my

Received: 6 August 2025; Revised: 21 January 2026; Accepted: 1 March 2026; Published: 28 April 2026

Abstract

This study explores the efficacy of copper-modified carbon adsorbent derived from *Samanea saman* (Cu^{2+}-SSCA) for the removal of metformin (MET), a commonly detected pharmaceutical pollutant, from aqueous environments. The pristine SSCA was synthesized through pyrolysis of the precursor under nitrogen (N_2), followed by CO_2 activation in a vertical furnace. Subsequent surface modification was achieved via impregnation with copper (II) nitrate [$Cu(NO_3)_2$], yielding the Cu^{2+}-SSCA. The resulting material demonstrated a Brunauer–Emmett–Teller surface area ($S.A._{BET}$) of 748.66 m^2/g, a mesoporous surface area ($S.A._{MESO}$) of 548.74 m^2/g, total pore volume (T.P.V.) of 0.3051 cm^3/g, followed by an average pore diameter (A.P.D.) of 2.41 nm, characteristics indicative of a well-developed mesoporous network. Process optimization using response surface methodology (RSM) identified optimum conditions at an activation temperature of 579 °C, followed by activation time of 1.20 h, and lastly, a Cu^{2+} ion impregnation ratio (IR) of 0.50 g/g. Under these conditions, the model-predicted MET adsorption capacity and Cu^{2+}-SSCA yield were 67.63 mg/g and 32.81%, respectively, in close agreement with experimental results of 68.90 mg/g (error of 1.84%) and 34.00% (error of 3.50%). Isotherm modelling revealed that MET adsorption adhered to the Langmuir model, exhibiting a Langmuir capacity (Q_m) of 109.27 mg/g. The Freundlich heterogeneity index (n_F) of 1.71 further confirmed favourable adsorption behaviour. In terms of kinetic study, the adsorption system followed pseudo-first order (PFO) the best.

Keywords: adsorption, surface modification, activated carbon, optimization, isotherm

Introduction

Pharmaceutical compounds are increasingly identified as emerging micropollutants with the ability to disturb aquatic ecosystems by impacting both plant and animal life. When present in water sources, even at minimal concentrations, these substances can threaten ecological stability and may pose long-term risks to human health and water quality [1]. Due to inefficient absorption in the digestive tract, nearly 90% of pharmaceutical compounds consumed by humans are expelled through urine and feces. These unmetabolized residues often end up in agricultural by-products or are released into wastewater networks, contributing to environmental pollution [2]. Pharmaceutical compounds administered for medical purposes frequently enter wastewater and sewage sludge produced by treatment facilities. However, most conventional wastewater treatment plants (WWTPs) lack the capability to effectively eliminate or break down these substances, resulting in their continuous release through treated effluents and buildup in sludge. Metformin (MET) is a widely prescribed oral medication for managing type 2 diabetes mellitus and is considered the first-line therapeutic option. It is chemically derived from guanidine, a bioactive component found in *Galega officinalis*, a traditional European medicinal herb historically used to address diabetic symptoms [3]. MET has been detected at measurable levels in various environmental matrices, including municipal and hospital wastewater, treatment plant sludge, tap water, and lake sediments. Its presence in aquatic systems has been reported across 14 different countries, highlighting its widespread environmental occurrence [4]. MET has been identified as hazardous to aquatic ecosystems, with exposure leading to stunted growth in the aquatic plant *Lemna minor* (evidenced by reduced leaf production) and reproductive disturbances in the freshwater crustacean *Daphnia*. These effects indicate the compound's potential to disrupt key biological functions in aquatic organisms [3].

A variety of treatment technologies have been utilized to remove pharmaceutical pollutants from wastewater, each with its own set of strengths and drawbacks. For instance, despite excellent MET degradation via poly(3,4-ethylenedioxythiophene) based photo-catalytic oxidation, the main drawback of this method is the gradual loss of catalyst conductivity and activity upon reuse, which requires chemical regeneration and limits long term operational stability [5]. Similarly, although hydroxyl radical based photochemical oxidation demonstrates effective MET degradation, its main drawback lies in the moderate removal efficiency together with high energy and oxidant demand, leading to increased operational cost and process complexity [6]. Furthermore, despite achieving high MET removal through integrated electrochemical and biological treatment, the main drawback of this approach is the requirement for multi stage processing involving energy intensive electrochemical oxidation followed by microbial adaptation, which prolongs treatment time and increases operational complexity [7]. Among these approaches, adsorption stands out for its effectiveness, leveraging surface interactions to trap a broad spectrum of contaminants, including heavy metals [8], pharmaceutical compounds [9], pesticide [10], synthetic dyes [11], carbon dioxide, CO_2 gas [12] and so on. This technique is widely preferred due to its simplicity, excellent removal performance, and cost-effectiveness [13]. Conventional activated carbon (AC) used in adsorption processes is typically derived from coal, a non-renewable resource linked to environmental issues and significant manufacturing expenses. As a sustainable alternative, growing interest has shifted toward utilizing agricultural waste materials like rice husks [14], orange peel [15], mango trunk [16], sludge biomass [17], sugarcane bagasse [18], alpinia galanga stem [19] and various other agricultural residues as eco-friendly and renewable sources for producing AC.

Enhancing the production of AC has become a key research focus, driven by the numerous variables that influence its performance. To address this complexity, response Surface Methodology (RSM) provides a robust statistical framework for optimizing parameters and accurately modelling process behaviour [20]. Central Composite Design (CCD) is one of the most commonly applied techniques within RSM, valued for its ability to reduce the number of required experiments, identify interactions between variables, and develop reliable predictive models. The use of three-dimensional (3D) response plots helps visualize the influence of different parameters, while Analysis of Variance (ANOVA) is employed to measure the model's precision and statistical relevance [21].

AC was selected as the base adsorbent because it is among the most reliable and widely applied materials for water purification. Its high specific surface area, adjustable pore structure, and rich surface functional groups enable efficient adsorption of a wide range of organic and inorganic contaminants, including emerging pharmaceutical compounds such as MET. AC itself is not a new material. However, the novelty of this study lies in the development of a copper (Cu^{2+})-modified AC and the systematic optimization of its synthesis parameters for MET removal. Metal modification is an effective strategy to enhance adsorption performance by introducing positively charged active sites and promoting specific interactions between metal centers and pollutant molecules without requiring severe thermal or chemical activation conditions. Previous studies have shown that Cu^{2+} successfully increased the removal of emerging contaminants by 25.99 % [15] and 30.40 % [22]. Positively charged metals attract pollutant molecules, with Cu^{2+} being widely used for its strong binding ability and lower cost compared to metals such as platinum or silver [21].

Samanea saman was selected as the biomass precursor for AC production due to its abundant availability, rapid growth, and high lignocellulosic content, making it a renewable and low-cost carbon source. The species, commonly known as the rain tree, was introduced to peninsular Malaysia in the early 20th century for landscaping and shading purposes [23] and is now widely planted in urban parks, roadsides, and institutional areas. Large quantities of *Samanea saman* biomass are generated through routine pruning activities, and much of this waste is commonly discarded or sent to landfills. Urban tree waste, including *Samanea saman* generated in the Klang Valley, is estimated to range between 300 to 500 tons annually [24]. Periodic pruning is necessary due to the large canopy size, which may pose safety risks to the surroundings [25]. Beyond its availability, *Samanea saman* possesses a hardwood structure, high fixed carbon content, and low ash composition below 5%, which makes it highly suitable for producing stable and high-quality carbon adsorbent. These characteristics distinguish *Samanea saman* as a promising and sustainable precursor for AC production. Therefore, the objective of this study is to develop and optimize a Cu^{2+}-modified carbon adsorbent derived from *Samanea saman* (Cu^{2+}-SSCA) for high-efficiency MET removal, and to apply RSM to optimize synthesis conditions and establish statistically validated process parameters and adsorption performance.

Materials and Methods

Precursor, chemicals and gases

Limb-derived raintree wood (*Samanea saman*) was sourced from Gombak, Selangor, and served as the main precursor material. Metformin (MET) in powder form and copper nitrate, $Cu(NO_3)_2$ (99.99% purity), were procured from Sigma-Aldrich. High-purity nitrogen (N_2) and carbon dioxide (CO_2) gases (99.99%

purity) were provided by MOX Gases Berhad, Malaysia.

Synthesis of Cu^{2+}-SSCA

The raw precursor was thoroughly washed to remove surface contaminants, then chopped into small fragments (approximately 1–1.5 cm). It was oven-dried at 60 °C for 24 hours, weighed, and positioned in a vertical furnace. Pyrolysis was conducted at 550 °C for 2 hours under a steady nitrogen (N_2) flow to produce char. Activation of the char was then carried out with carbon dioxide (CO_2) under various conditions, with activation temperatures extending from 432 to 768 °C and durations from 0.32 to 3.68 hours, resulting in pristine SSCA. To modify the surface, the pristine SSCA was impregnated with Cu^{2+} ions using copper nitrate ($Cu(NO_3)_2$), with impregnation ratios (IR) varying between 0 and 2.51 g/g. The activation parameters and IR values were generated using RSM and are detailed in Table 1. The IR was calculated as follows:

$$IR\ \left(\frac{g}{g}\right) = \frac{W_{Cu}\,(g)}{W_p\,(g)} \quad (1)$$

where W_{Cu} denotes to the weight of $Cu(NO_3)_2$ salt and W_p represents to the weight of precursor.

Optimization investigation

To optimize the synthesis process, the dataset was analyzed via Response Surface Methodology (RSM) which was executed to explore the impact of three variables: activation temperature (X_1), activation time (X_2), and impregnation ratio (IR, X_3). Two key responses were measured: the adsorption capacity for MET (Y_1) and the yield of Cu^{2+}- SSCA (Y_2). Every variable was studied at five levels: +α, +1, 0, -1, and -α, corresponding to activation temperatures of 432, 500, 600, 700, and 768 °C; activation times of 0.32, 1.00, 2.00, 3.00, and 3.68 hours; and IR values of 0.00, 0.50, 1.25, 2.00, and 2.51 g/g. The yield of Cu^{2+}-SSCA was determined via the subsequent equation:

$$Yield\ (\%) = \frac{W_{Cu^{2+}-SSAC}}{W_p} \quad (2)$$

where $W_{Cu2+\text{-}SSCA}$ is the dry weight of Cu^{2+}-SSCA, whilst W_p refers to the dry weight of precursor.

Characterization methods

The study conducted an in-depth characterization of the physicochemical properties of the samples, focusing on surface area parameters such as BET surface area ($S.A._{BET}$) and mesopore surface area ($S.A._{MESO}$), as well as pore characteristics including total pore volume (T.P.V.) and average pore diameter (A.P.D.). These textural properties were analyzed using a Micromeritics ASAP 2010 volumetric adsorption analyzer based on the Brunauer–Emmett–Teller (BET) method. Elemental composition—including carbon, hydrogen, nitrogen, and sulfur content—was determined using a Perkin Elmer Series II 2400 elemental analyzer (USA), offering insights into the chemical structure of the adsorbents. Additionally, proximate analysis was conducted to evaluate moisture content, volatile matter, fixed carbon, and ash content. This analysis helps assess the thermal stability and carbon richness of the material, which are critical for adsorption efficiency and structural integrity during high-temperature treatments.

Isotherm investigation

For the isotherm study, six individual Erlenmeyer flasks were prepared, each containing MET solutions with different starting concentrations (C_0) of 10 – 100 mg/L. The flasks were positioned in a thermostatic shaking water bath and agitated under controlled conditions. Each experiment involved 200 mL of MET solution, 0.20 g of the optimized Cu^{2+}-SSCA adsorbent, and a constant temperature of 30 °C. After reaching adsorption equilibrium, the residual MET concentration (C_e) in the solution was quantified with a UV-Vis spectrophotometer (Agilent Cary 60, USA). The equation presented below was used to compute the equilibrium adsorption capacity (q_e, mg/g):

$$q_e = \frac{(C_o - C_e)V}{W} \quad (3)$$

The experimental data were analysed using numerous isotherm models to evaluate the adsorption behaviour, and the respective equations for each model are provided below:

Langmuir [26]:

$$q_e = \frac{Q_m K_L C_e}{1 + K_L C_e} \quad (4)$$

Freundlich [27]:

$$q_e = K_F C_e^{1/n_F} \quad (5)$$

Temkin [28]:

$$q_e = \frac{RT}{B}\ln(AC_e) \quad (6)$$

the constants in these isotherm models are clearly described and detailed in the study by [29].

Kinetic investigation

A similar experiment to the isotherm study was performed, but instead of taking concentration readings only at equilibrium, measurements were taken at several time intervals until equilibrium was reached to study the kinetic behaviour. Two kinetic models were used as follows:

Pseudo-first order (PFO) [30]:

$$q_t = q_e[1 - exp(-k_1 t)] \quad (7)$$

Pseudo-second order (PSO) [31]:

$$q_t = \frac{k_2 q_e^2 t}{1 + k_2 q_e t} \quad (8)$$

the constants involved in these kinetic models are clearly defined and described in detail in the study reported in [29].

Results and Discussion

Optimization process: Regression models development

Table 1 presents the complete experimental design, detailing both the variables and responses associated with Cu^{2+}-SSCA production, as established through RSM. The observed adsorption capacity for MET ranged from 51.40 to 74.00 mg/g, while the material yield spanned from 21.47% to 39.71%. The material yield within this range was considered high compared to other biomass yields, such as hazelnut shells, which ranged from 8.70% to 20.50% [32], cassava stem, which ranged from 3.80% to 30.20% [33], and coconut waste, which ranged from 14.23% to 32.82% [34]. The software selected quadratic models based on the coded input variables, providing dependable mathematical predictions for the outcomes based on the experimental parameters, as elaborated below:

MET uptakes (%), Y_1:

$$Y_1 = 71.50 + 4.72X_1 - 2.32X_2 + 2.51X_3 + 1.12X_1X_2 - 2.04X_1X_3 + 0.855X_2X_3 - 3.31{X_1}^2 - 1.53{X_2}^2 - 1.53{X_3}^2 \quad (9)$$

Cu^{2+}-SSCA yield (%), Y_2:

$$Y_2 = 27.18 - 4.48X_1 + 1.85X_2 - 2.96X_3 - 0.6625X_1X_2 + 0.81X_1X_3 + 0.955X_2X_3 + 0.7482{X_1}^2 + 0.2285{X_2}^2 + 2.20{X_3}^2 \quad (10)$$

The regression graphs in **Figures 1(a)** and **1(b)** depict the relationship between forecasted data and observed measurements for MET removal and Cu^{2+}-SSCA production, respectively. The R^2 and adjusted R^2 values 0.9506 and 0.9060 for MET uptake, and 0.9311 and 0.8692 for yield which indicate an excellent model fit, capturing a substantial portion of response variability with strong statistical validity.

The low standard deviations (S.D.) of 1.92 for MET uptake and 1.98 for Cu^{2+}-SSCA yield highlight the precision and consistency of the models, suggesting minimal prediction error across all experiments. Additionally, the adequate precision (A.P.) values of 14.68 and 13.26 for MET uptake and Cu^{2+}-SSCA yield, respectively, far exceed the threshold of 4, confirming robust signal-to-noise ratios and the models' overall reliability in predicting outcomes within the defined design space [35].

Table 1. Variables and responses for Cu^{2+}-SSCA production as generated by RSM

Run	Cu^{2+}-SSCA Preparation Variables			Responses	
	Activation Temperature, X_1 (°C)	Activation Time, X_2 (minutes)	IR, X_3 (g/g)	MET Uptakes, Y_1 (mg/g)	Cu^{2+}-SSCA Yield, Y_2 (%)
1	500 (-1)	3.00 (+1)	0.50 (-1)	51.40	37.94
2	700 (+1)	1.00 (-1)	2.00 (+1)	70.90	23.24
3	600 (0)	2.00 (0)	1.25 (0)	72.64	25.59
4	600 (0)	2.00 (0)	1.25 (0)	71.81	25.00
5	432 (-α)	2.00 (0)	1.25 (0)	55.27	37.94
6	700 (+1)	3.00 (+1)	2.00 (+1)	70.67	25.00
7	600 (0)	2.00 (0)	1.25 (0)	74.00	30.88
8	600 (0)	3.68 (+α)	1.25 (0)	62.78	32.06
9	600 (0)	2.00 (0)	2.51 (+α)	71.43	27.94
10	500 (-1)	1.00 (-1)	2.00 (+1)	66.95	26.76
11	768 (+α	2.00 (0)	1.25 (0)	68.85	21.47
12	700 (+1)	3.00 (+1)	0.50 (-1)	68.00	28.53
13	600 (0)	2.00 (0)	1.25 (0)	73.70	26.76
14	600 (0)	2.00 (0)	1.25 (0)	68.85	28.53
15	600 (0)	2.00 (0)	1.25 (0)	68.01	26.18
16	500 (-1)	1.00 (-1)	0.50 (-1)	59.52	37.35
17	700 (+1)	1.00 (-1)	0.50 (-1)	71.88	26.76
18	600 (0)	2.00 (0)	0.00 (-α)	62.78	39.71
19	500 (-1)	3.00 (+1)	2.00 (+1)	62.02	35.00

20	600 (0)	0.32 (-α)	1.25 (0)	71.43	24.41

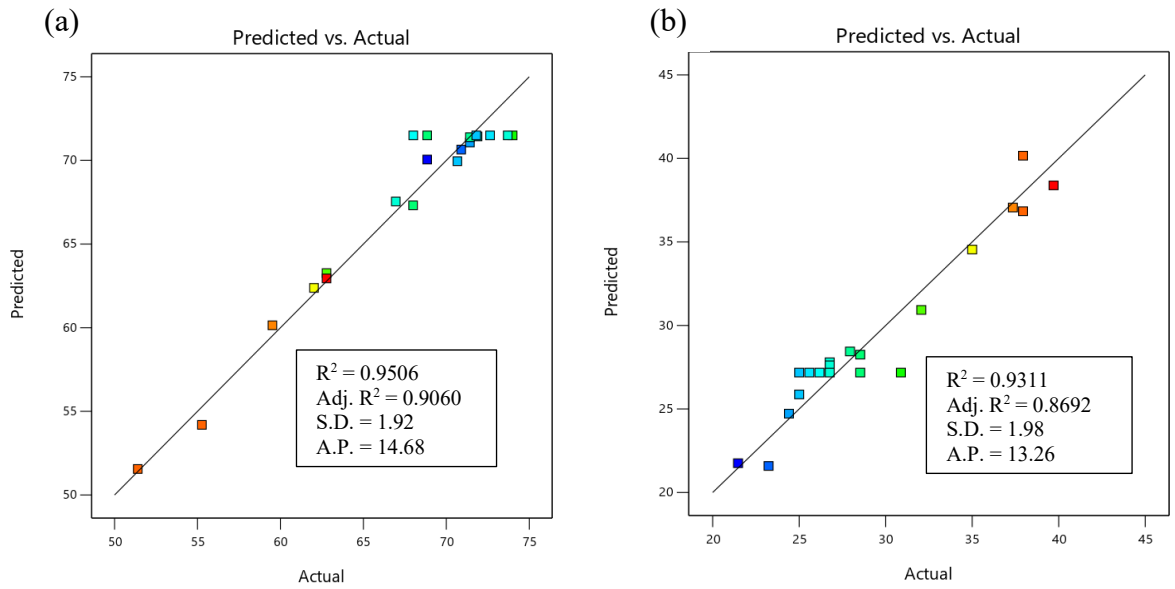

Figure 1. Regression plots of predicted versus actual for (a) MET uptake and (b) Cu^{2+}-SSCA yield

ANOVA results

Table 2 provides a comprehensive overview of the ANOVA findings for MET adsorption and Cu^{2+}-SSCA yield. Both responses exhibited strong statistical significance, with p-values of < 0.0001 for MET uptake and 0.0001 for yield, confirming the robustness and reliability of the developed models. For MET uptake, the influential terms were X_1, X_2, X_3, X_1X_3, X_1^2, X_2^2, and X_3^2, while Cu^{2+}-SSCA yield was significantly affected by X_1, X_2, X_3, and X_3^2. The F-values further reinforce the dominant effect of activation temperature and IR on both responses. Notably, MET uptake was primarily governed by activation temperature (F = 130.62) and IR (F = 30.15), whereas Cu^{2+}-SSCA yield also showed strong dependence on activation temperature (F = 69.94) and IR (F = 30.42). These findings highlight the critical influence of these two parameters in maximizing both the adsorptive efficiency and material yield of the synthesized carbon.

Three-dimensional (3D) surface plot

Figure 2(a) presents a three-dimensional surface plot illustrating the combined effects of activation temperature and IR on MET adsorption, while **Figure 2(b)** shows their influence on Cu^{2+}-SSCA yield. The highest MET uptake, reaching 74.00 mg/g, occurred at an elevated activation temperature of 650 °C and an IR of 1.40 g/g. This higher temperature enhanced the elimination of volatile compounds, promoting the development of well-structured pores and increasing surface area—factors that collectively boosted adsorption performance [36]. Additionally, it contributed to the thermal breakdown of lightweight hydrocarbons, leading to improved carbonization and more pronounced porosity [37]. A higher IR increased the surface loading of Cu^{2+} ions, thereby enhancing electrostatic interactions and complexation with MET molecules, further improving the adsorptive efficiency. Conversely, the lowest MET uptake of 51.40 mg/g was observed at the lowest tested conditions—500 °C activation temperature and an IR of 0.50 g/g. These insufficient parameters limited pore development and reduced the presence of surface-bound Cu^{2+} ions, thereby weakening interactions with MET molecules. Moreover, activation temperatures exceeding 650 °C led to structural pore collapse and diminished surface area, slightly reducing MET adsorption capacity [38]. Similarly, IR values above 1.40 g/g caused excessive Cu^{2+} deposition, which obstructed pore access and further inhibited adsorption efficiency [22].

As shown in **Figure 2(b)**, the lowest Cu^{2+}-SSAC yield of 21.47% occurred under the highest activation temperature and IR conditions, underscoring their adverse effect on material yield. Increasing the activation temperature from 500 to 700 °C intensified pyrolytic decomposition, leading to substantial volatilization and elemental loss, thereby reducing the final yield [21]. Likewise, higher IR levels introduced excess Cu^{2+} ions, which accelerated burn-off and further diminished the carbon content. These findings emphasize the importance of carefully optimizing both activation temperature and impregnation ratio to maintain a balance between desirable porosity and acceptable material yield.

Table 2. ANOVA results for MET uptakes and Cu^{2+}-SSCA yield responses

Source	Response 1, Y_1: MET uptakes by Cu^{2+}-SSCA				
	Sum of Squares	**DF**	**Mean Square**	**F Value**	**p-value**
Model	709.43	9	78.83	21.36	< 0.0001
X_1	303.67	1	303.67	82.28	< 0.0001
X_2	73.62	1	73.62	19.95	0.0012
X_3	86.08	1	86.08	23.33	0.0007
X_1X_2	9.99	1	9.99	2.71	0.1309
X_1X_3	33.46	1	33.46	9.07	0.0131
X_2X_3	5.85	1	5.85	1.58	0.2367
X_1^2	158.25	1	158.25	42.88	< 0.0001
X_2^2	33.74	1	33.74	9.14	0.0128
X_3^2	33.74	1	33.74	9.14	0.0128

Source	Response 2, Y_2: Cu^{2+}-SSCA yield				
	Sum of Squares	**DF**	**Mean Square**	**F Value**	**p-value**
Model	530.59	9	58.95	15.03	0.0001
X_1	274.42	1	274.42	69.94	< 0.0001
X_2	46.59	1	46.59	11.87	0.0063
X_3	119.36	1	119.36	30.42	0.0003
X_1X_2	3.51	1	3.51	0.8949	0.3665
X_1X_3	5.25	1	5.25	1.34	0.2743
X_2X_3	7.30	1	7.30	1.86	0.2026
X_1^2	8.07	1	8.07	2.06	0.1821
X_2^2	0.7522	1	0.7522	0.1917	0.6708
X_3^2	70.06	1	70.06	17.85	0.0018

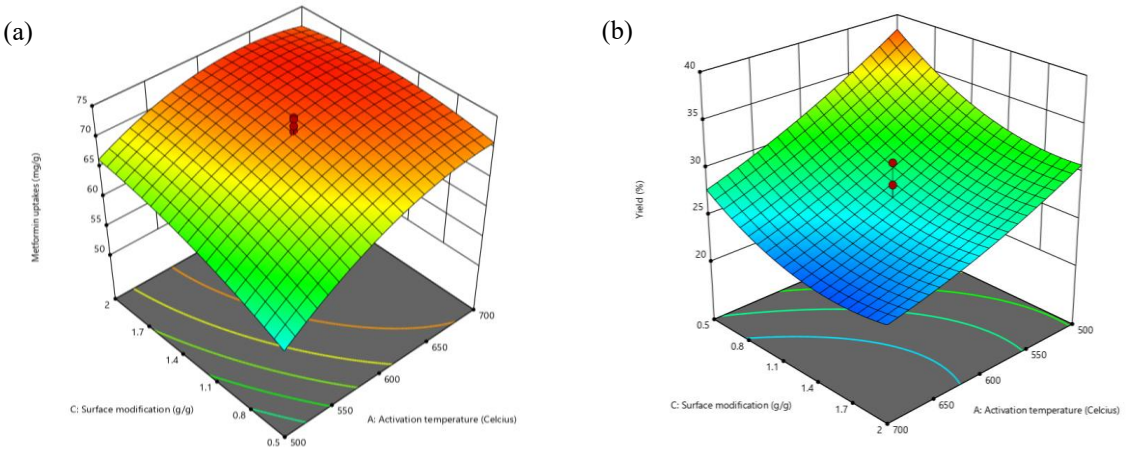

Figure 2. 3D surface plots for (a) MET uptake and (b) Cu^{2+}-SSCA yield responses

Optimal conditions and model validation

Table 3 presents the optimized preparation conditions and corresponding model validation results. The optimal process settings were determined by minimizing input variables while maximizing the desired responses. Through RSM optimization, the predicted optimum conditions were 579 °C for activation temperature, 1.20 hours for activation time, and an IR of 0.50 g/g. Under these parameters, the model forecasted a MET uptake of 67.63 mg/g and a Cu^{2+}-SSCA yield of 32.81%. This yield is considered high in comparison with other optimized carbon adsorbents derived from biomass, such as merbau sawdust of 31.80% [39], coconut waste of 25.70% [34] and *Tecoma* chip wood of 27.68% [40]. Experimental validation produced slightly higher values of 68.90 mg/g and 34.00%, respectively, corresponding to low error margins of 1.84% and 3.50%. The close alignment well within the acceptable 10% error threshold demonstrates the high accuracy, robustness, and predictive strength of the developed models [41].

Table 3. Optimum conditions and model validation

Optimum Variables			Optimum Responses					
			MET Uptakes, Y_1			Cu^{2+}-SSCA Yield, Y_2		
X_1 (°C)	X_2 (hours)	X_3 (g/g)	Predicted (mg/g)	Actual (mg/g)	Error (%)	Predicted (%)	Actual (%)	Error (%)
579	1.20	0.50	67.63	68.90	1.84	32.81	34.00	3.50

X_1 = activation temperature; X_2 = activation time; X_3 = IR

Table 4. Surface area and pore characteristics

Samples	$S.A._{BET}$ (m^2/g)	$S.A._{MESO}$ (m^2/g)	T.P.V. (cm^2/g)	A.P.D. (nm)
Precursor	4.11	-	0.0001	-
Pristine SSCA	761.41	562.86	0.3074	2.44
Cu^{2+}-SSCA	748.66	548.74	0.3051	2.41

Characteristics of samples

Surface area and pores characteristic

Table 4 compiles the surface area and porosity characteristics of the precursor, pristine SSCA, and Cu^{2+}-SSCA materials. The precursor displayed a very low BET surface area ($S.A._{BET}$) of 4.11 m^2/g, and total pore volume (T.P.V.) of 0.0001 cm^3/g, suggesting negligible porosity. During carbonization, dehydration and the expulsion of light volatile components primarily cellulose and hemicellulose initiated the formation of pore structures. This was further enhanced during physical activation at elevated temperatures, where the breakdown of denser compounds, such as hemicellulose-lignin complexes, occurred. Concurrently, interaction with CO_2 gas contributed to the enlargement and increased density of pore channels. Consequently, the pristine SSCA exhibited significantly enhanced porosity, with a $S.A._{BET}$ of 761.41 m^2/g, $S.A._{MESO}$ of 562.86 m^2/g, T.P.V. of 0.3074 cm^3/g, and an average pore diameter (A.P.D.) of 2.44 nm, confirming a predominantly mesoporous structure. After surface modification with $Cu(NO_3)_2$, slight reductions in $S.A._{BET}$, $S.A._{MESO}$, T.P.V., and A.P.D. were observed dropping to 748.66 m^2/g, 548.74 m^2/g, 0.3051 cm^3/g, and 2.41 nm, respectively due to partial pore obstruction and surface coverage by deposited copper salts.

Results on elemental analysis and proximate analysis

Table 5 provides a comprehensive summary of the proximate and elemental analysis results for the examined samples. *Samanea saman* demonstrated a remarkably high fixed carbon content of 27.61%, notably exceeding values reported for other biomass sources such as rice husk (13.82%), corn straw (14.12%), wood dust (14.46%), and coconut shell (18.86%) [42]. This exceptional carbon richness validates its selection as a suitable precursor for Cu^{2+}-SSCA synthesis in this study. Initially, the raw precursor exhibited high moisture and volatile matter contents, which decreased substantially to 3.45% and 14.72%, respectively, after undergoing carbonization and activation [43]. In contrast, fixed carbon content increased markedly to 77.39%, enhancing the material's stability and adsorption potential. The final ash content in Cu^{2+}-SSCA remained low at 4.44%, which is advantageous since ash contributes little to adsorption [44]. Elemental analysis supported these findings, showing a rise in carbon content from 37.71% in the precursor to 78.31% in the final product. Meanwhile, elements associated with volatiles namely hydrogen, nitrogen, sulfur, and oxygen declined significantly due to thermal decomposition and volatilization.

Table 5. Elemental and proximate analysis of samples

Samples	Elemental Analysis (%)					Proximate Analysis (%)			
	C	H	N	S	*O+	Moisture	Volatile matter	Fixed carbon	Ash
Precursor	37.71	5.67	0.91	0.31	55.4	12.61	56.51	27.61	3.27
Pristine SSCA	81.14	4.32	0.66	0.23	13.65	3.39	14.93	78.19	3.49
Cu^{2+}-SSCA	78.31	4.26	0.66	0.25	16.52	3.45	14.72	77.39	4.44

Adsorption isotherm

Table 6 provides a detailed summary of the isotherm model fitting results. Among the evaluated models, the Langmuir isotherm exhibited the best agreement with the experimental data for MET adsorption onto Cu^{2+}-SSCA. This was supported by the lowest RMSE of 1.29 and a minimal error margin of 5.67%, indicating strong predictive accuracy. In the literature, the Langmuir model has also been reported to suitably describe MET adsorption by corn straw based biochar [45], natural zeolite [3] and water hyacinth based AC [46]. The superior fit implies that the adsorption process adheres to a monolayer mechanism, likely dominated by specific binding interactions between MET molecules and surface-bound Cu^{2+} ions. The Freundlich heterogeneity factor (n_F), ranging from 1 to 10, further confirms the favourability and efficiency of the adsorption. Additionally, the Langmuir model estimated a maximum adsorption capacity (Q_m) of 109.27 mg/g, substantially outperforming orange peel-derived AC, which reported only 50.99 mg/g for MET removal [47], chichá-do-cerrado fruit shells based AC at 45.39 mg/g [48] and iron-biochar composite at 15.20% [49].

Adsorption kinetic

Table 7 presents the summary of the kinetic results. The average error for the PFO model was 7.38%, which is lower than that of the PSO model (8.87%), confirming that MET adsorption onto Cu^{2+}-SSAC is better described by the PFO model. This indicates that the adsorption process is predominantly governed by surface-site interactions, where MET molecules occupy available active sites on the Cu^{2+}-SSAC surface, with the overall rate influenced by the transfer of MET molecules from the bulk solution to the adsorbent surface [50]. As the initial MET concentration increased from 10 to 100 mg/L, both rate constants k_1 and k_2 decreased from 0.95 to 0.64 h^{-1} and from 0.11 to 0.007 g/mg.h, respectively. This decline can be attributed to the higher availability of MET molecules at elevated concentrations, which intensifies competition for active adsorption sites. In contrast, at lower initial concentrations, fewer MET molecules are present, resulting in reduced competition and faster adsorption. Consequently, the reaction rate is higher at lower concentrations and gradually decreases as adsorption sites become increasingly contested at higher concentrations [43].

Conclusion

This study successfully developed a Cu^{2+}-SSCA and demonstrated its strong potential for the removal of MET from aqueous environments. The optimization strategy based on RSM proved effective in identifying suitable preparation conditions and confirmed the reliability of the developed predictive models. The synthesized adsorbent exhibited a well-developed mesoporous structure and favourable surface characteristics, which contributed to its high affinity toward MET molecules. Adsorption behaviour was consistent with monolayer uptake on a homogeneous surface, while kinetic evaluation indicated that the adsorption process was governed primarily by surface interaction mechanisms. These findings confirm that copper modification enhances the adsorption performance of biomass derived carbon and supports its applicability as a promising low-cost material for pharmaceutical pollutant removal from water. Overall, the present work provides valuable insight into the design of metal modified carbon adsorbents for wastewater treatment applications and offers a practical foundation for future scale up, continuous flow studies, and further investigation of multicomponent adsorption systems in complex wastewater matrices.

Table 6. Isotherm parameters for MET-Cu^{2+}-SSCA adsorption system at 30°C

Langmuir	Values	Freundlich	Values	Temkin	Values
Q_m (mg/g)	109.27	n_F	1.71	A_T (L/mg)	0.96
K_L (L/mg)	0.056	K_F (mg/g)(L/mg)$^{1/n}$	9.72	B_T (L/mg)	19.10
RMSE	1.29	RMSE	2.55	RMSE	4.61
Error (%)	5.67	Error (%)	8.68	Error (%)	21.40

Table 7. Kinetic parameters for MET-Cu^{2+}-SSCA adsorption system at 30°C

Initial Concentration (mg/L)	PFO				PSO			
	q_e, calculated (mg/g)	q_e, actual (mg/g)	k_1 (h^{-1})	Error (%)	q_e, calculated (mg/g)	q_e, actual (mg/g)	K_2 (g/mg.h)	Error (%)
10	8.36	7.72	0.95	9.48	1.32	8.79	0.11	9.36
20	16.32	14.5	0.81	8.84	19.79	16.88	0.05	9.62
40	31.54	27.77	0.75	8.71	38.59	32.13	0.02	10.28
60	47.22	40.78	0.66	4.47	59.80	46.48	0.01	6.50
80	60.94	51.68	0.68	8.20	77.40	59.89	0.008	10.74

100	70.29	59.77	0.64	4.60	89.74	68.90	0.007	6.70
Average				7.38				8.87

Acknowledgements
This research is supported by Malaysian Ministry of Higher Education under the Prototype Research Grant Scheme (project code: PRGS/1/2025/TK/USM/01/1).

References

1. Mat Zaini, Y. M., Dina Amalia Purba, L., Abdullah, N., Yuzir, A., Iwamoto, K., and Mohamad, S. E. (2022). Removals of atenolol, gliclazide and prazosin using sequencing batch reactor. *Materials Today: Proceedings,* 65: 3007-3014.
2. Mohamad, F. M. Y., Abdullah, A. Z., and Ahmad, M. A. (2024). Amoxicillin adsorption from aqueous solution by Cu(II) modified lemon peel based activated carbon: Mass transfer simulation, surface area prediction and F-test on isotherm and kinetic models. *Powder Technology,* 438: 119589.
3. Ferri, B. B., Wernke, G., Resende, J. F., Ribeiro, A. C., Cusioli, L. F., Bergamasco, R., and Vieira, M. F. (2024). Natural zeolite as adsorbent for metformin removal from aqueous solutions: Adsorption and regeneration properties. *Desalination and Water Treatment,* 320: 100602.
4. Ambrosio-Albuquerque, E. P., Cusioli, L. F., Bergamasco, R., Sinópolis Gigliolli, A. A., Lupepsa, L., Paupitz, B. R., Barbieri, P. A., Borin-Carvalho, L. A., and de Brito Portela-Castro, A. L. (2021). Metformin environmental exposure: A systematic review. *Environmental Toxicology and Pharmacology,* 83: 103588.
5. Kumar, R., Akbarinejad, A., Jasemizad, T., Fucina, R., Travas-Sejdic, J., and Padhye, L. P. (2021). The removal of metformin and other selected PPCPs from water by poly(3,4-ethylenedioxythiophene) photocatalyst. *Science of The Total Environment,* 751: 142302.
6. Garazade, N., Can-Güven, E., Güven, F., Yazici Guvenc, S., and Varank, G. (2025). Application of machine learning algorithms for the prediction of metformin removal with hydroxyl radical-based photochemical oxidation and optimization of process parameters. *Journal of Hazardous Materials,* 489: 137552.
7. Hosseini, M. M., Solouki, M., Ghobadi-Nejad, Z., and Yaghmaei, S. (2026). Integrated Electrochemical–Biological Treatment for Efficient Removal of Metformin and Its By-Products: Optimization, Mineralization, and Toxicity Assessment. *Case Studies in Chemical and Environmental Engineering*: 101322.
8. Khir, N. H. M., Salleh, N. F. M., Ghafar, N. A., Shukri, N. M., and Jusoh, R. (2025). Preparation and characterization of modified rambutan peels for the removal of chromium(VI) and nickel(II) from aqueous solution: Environmental impact and optimization *Malaysian Journal of Analytical Sciences,* 29(1): 1292.
9. Ramlee, D. A., Nordin, N. A., Rahman, N. A., and Bahruji, H. (2024). Removal of acetaminophen by using electrospun pan/sago lignin-based activated carbon nanofibers. *Malaysian Journal of Analytical Sciences,* 28(6): 1442 - 1457.
10. Aziz, A., Nasehir Khan, M. N., Mohamad Yusop, M. F., Mohd Johan Jaya, E., Tamar Jaya, M. A., and Ahmad, M. A. (2021). Single-stage microwave-assisted coconut-shell-based activated carbon for removal of dichlorodiphenyltrichloroethane (DDT) from aqueous solution: Optimization and batch studies. *International Journal of Chemical Engineering,* 2021(1): 9331386.
11. Gunasekaran, S., Liu, A. J. X., and Ng, S. L. (2024). Activated carbon/iron oxide composites with different weight ratios for acid orange 7 removal. *Malaysian Journal of Analytical Sciences,* 28(6): 1359 - 1373.
12. Nur Syahirah Mohamed, H., Farihahusnah, H., Lai Ti, G., and Mohamed Kheireddine, A. (2024). Characterisation of egg white-impregnated activated carbon for CO2 adsorption application. *Malaysian Journal of Science,* 43(Sp1): 20-25.
13. Yusop, M. F. M., Tamar Jaya, M. A., Idris, I., Abdullah, A. Z., and Ahmad, M. A. (2023). Optimization and mass transfer simulation of remazol brilliant blue R dye adsorption onto meranti wood based activated carbon. *Arabian Journal of Chemistry,* 16: 104683.
14. Saputra, D. A., Pratoto, A., Rahman, M. F., and Kodama, A. (2024). The effect of chemical activation agents and activation temperature on the pore structure of rice husk-derived activated carbon. *Malaysian Journal of Science,* 43(Sp1): 1-7.
15. Firdaus, M. Y. M., Rashid, M. M., Alam, M. M., and Ahmad, M. A. (2025). Copper-modified surface of orange peel-derived activated carbon for amoxicillin removal: Mass transfer simulation, attraction mechanism, and regeneration studies. *Arabian Journal for Science and Engineering*.
16. Firdaus, M. Y. M., Rashid, M. M., Alam, M. M., and Ahmad, M. A. (2025). Enhanced Cd2+ removal via deprotonated-mango trunk functionalized carbon: Optimization and F-test for linear and non-linear isotherm and kinetic models. *Chemical Engineering Research and Design,* 220: 96-116.
17. Ahmad, M. A., Yusop, M. F. M., Awang, S., Yahaya, N. K. E. M., Rasyid, M. A., and Hassan, H. (2021). Carbonization of sludge biomass of water treatment plant using continuous screw type conveyer pyrolyzer for methylene blue removal.

IOP Conference Series: Earth and Environmental Science, 765: 012112.
18. Zainuddin, N. J., Jamaluddin, M. A., Gusri, N. A., Rahizal, N. A., and Yusof, N. H. I. M. (2024). Optimization study of methylene blue decolorization using waterfilter prototype embedded with sugarcane bagasse biochar. *Malaysian Journal of Chemistry,* 26(3): 264-272.
19. Ahammad, N. A., Yusop, M. F. M., Mohd Din, A. T., and Ahmad, M. A. (2021). Preparation of alpinia galanga stem based activated carbon via single-step microwave irradiation for cationic dye removal. *Sains Malaysiana,* 50(8): 2251-2269.
20. Daouda, M. M. A., Akowanou, A. V. O. e., Mahunon, S. E. R., Adjinda, C. K., Aina, M. P. e., and Drogui, P. (2021). Optimal removal of diclofenac and amoxicillin by activated carbon prepared from coconut shell through response surface methodology. *South African Journal of Chemical Engineering,* 38(1): 78-89.
21. Yusop, M. F. M., Baharudin, M. H., Rashid, M. M., Alam, M. M., and Ahmad, M. A. (2025). Amoxicillin adsorption onto oil palm trunk-derived activated carbon: synthesis optimization, modelling of mass transfer and ultrasonic regeneration. *Journal of Chemical Technology & Biotechnology,* 100(6): 1310-1327.
22. Mohamad, F. M. Y., Rashid, M. M., Alam, M. M., and Ahmad, M. A. (2025). Copper metal-functionalized carbon from rattan waste via microwave pyrolysis for enhanced chloramphenicol removal: Optimization and F-test study. *Particuology,* 100: 196-213.
23. Tahir, Z. M., Mohamad Mohidin, F. S., and N Rosely, N. F. (2020). Visual Tree Analysis of Rain Trees (Samanea saman) in Universiti Sains Malaysia, Main Campus. *IOP Conference Series: Earth and Environmental Science,* 549(1): 012032.
24. Alli, H., and Hishammuddin, U. (2022). Investigation and Development of Raintree Furniture From The Waste of Urban Tree. *International Journal of Social Science Research,* 4(1): 34-45.
25. Fröhlich, A., Przepióra, F., Drobniak, S., Mikusiński, G., and Ciach, M. (2024). Public safety considerations constraint the conservation of large old trees and their crucial ecological heritage in urban green spaces. *Science of The Total Environment,* 948: 174919.
26. Langmuir, I. (1918). The adsorption of gases on plane surfaces of glass, mica and platinum. *Journal of the American Chemical Society,* 40(9): 1361-1403.
27. Freundlich, H. (1906). Over the adsorption in solution. *Journal of Physical Chemistry,* 57(385471): 1100-1107.
28. Tempkin, M., and Pyzhev, V. (1940). Kinetics of ammonia synthesis on promoted iron catalyst. *Acta Physicochimica URSS,* 12(1): 327.
29. Mohamad, F. M. Y., Abdullah, A. Z., and Ahmad, M. A. (2023). Adsorption of remazol brilliant blue R dye onto jackfruit peel based activated carbon: Optimization and simulation for mass transfer and surface area prediction. *Inorganic Chemistry Communications,* 158: 111721.
30. Lagergren, S. K. (1898). About the Theory of So-called Adsorption of Soluble Substances. *Sven. Vetenskapsakad. Handingarl,* 24: 1-39.
31. Ho, Y. S., and McKay, G. (1998). Sorption of dye from aqueous solution by peat. *Chemical Engineering Journal,* 70(2): 115-124.
32. Kılıç, M., Bekman, M. E., Bodur, F., Yıldız, A., and Varol, E. A. (2025). Modeling and optimization of flash heating process conditions for activated carbon production using Response Surface Methodology (RSM). *Diamond and Related Materials,* 154: 112239.
33. Sulaiman, N. S., Hashim, R., Mohamad Amini, M. H., Danish, M., and Sulaiman, O. (2018). Optimization of activated carbon preparation from cassava stem using response surface methodology on surface area and yield. *Journal of Cleaner Production,* 198: 1422-1430.
34. Sopandi, T. P., Sulianto, A. A., Anugroho, F., Yusoff, M. Z. M., Mohamed, M. S., Farid, M. A. A., and Setyawan, H. Y. (2025). RSM-optimized biochar production from young coconut waste (*Cocos nucifera*): Multivariate analysis of non-linear interactions between temperature, time, and activator concentration. *Industrial Crops and Products,* 223: 120157.
35. Beyan, S. M., Prabhu, S. V., Sissay, T. T., and Getahun, A. A. (2021). Sugarcane bagasse based activated carbon preparation and its adsorption efficacy on removal of BOD and COD from textile effluents: RSM based modeling, optimization and kinetic aspects. *Bioresource Technology Reports,* 14: 100664.
36. Yu, H., Mikšík, F., Thu, K., and Miyazaki, T. (2024). Characterization and optimization of pore structure and water adsorption capacity in pinecone-derived activated carbon by steam activation. *Powder Technology,* 431: 119084.
37. Weldekidan, H., Patel, H., Mohanty, A., and Misra, M. (2024). Synthesis of porous and activated carbon from lemon peel waste for CO_2 adsorption. *Carbon Capture Science & Technology,* 10: 100149.
38. Firdaus, M. Y. M., Nasran, M. N. K., Ridzuan, Z., Zuhairi, A. A., and Azmier, M. A. (2023). Mass transfer simulation on remazol brilliant blue R dye adsorption by optimized teak wood Based activated carbon. *Arabian Journal of Chemistry,* 16(6): 104780.
39. Yaacob, N. A., Khasri, A., Ridzuan, M. J. M., and Salleh, N. H. M. (2021). Statistical optimization of methylene blue dye removal efficiency by merbau based activated carbon via RSM-CCD. *AIP Conference Proceedings,* 2339(1): 020223.

40. Nasran, N. K. M., Firdaus, M. Y. M., Faizal, P. M. L. M., and Azmier, A. M. (2023). Alteration of Tecoma chip wood waste into microwave-irradiated activated carbon for amoxicillin removal: Optimization and batch studies. *Arabian Journal of Chemistry,* 16(10): 105110.
41. Yusop, M. F. M., Mohd Johan Jaya, E., Mohd Din, A. T., Bello, O. S., and Ahmad, M. A. (2022). Single-stage optimized microwave-induced activated carbon from coconut shell for cadmium adsorption. *Chemical Engineering & Technology,* 45(11): 1943-1951.
42. Wei, X., Huang, S., Yang, J., Liu, P., Li, X., Wu, Y., and Wu, S. (2023). Adsorption of phenol from aqueous solution on activated carbons prepared from antibiotic mycelial residues and traditional biomass. *Fuel Processing Technology,* 242: 107663.
43. Firdaus, M. Y. M., Rashid, M. M., Alam, M. M., and Ahmad, M. A. (2025). Synthesis of deprotonated grape stem functionalized carbon for boosted Cu^{2+} adsorption – Optimization, interaction mechanism, and F-test analysis. *Microchemical Journal,* 218: 115795.
44. Aziz, A., Mohamad Yusop, M. F., and Ahmad, M. A. (2024). Harnessing microwave energy to transform Nephelium lappaceum L. peel into activated carbon for chloramphenicol eradication in aqueous solutions. *Materials Chemistry and Physics,* 318: 129311.
45. Wu, W., Zhao, B., Qu, Z., Pan, J., and Guo, Q. (2025). Adsorption of metformin in aqueous system by biochars derived from different biomasses: Performance and mechanisms. *Colloids and Surfaces A: Physicochemical and Engineering Aspects,* 727: 138438.
46. Mohammad, A. H., Radovic, I., Ivanović, M., and Kijevčanin, M. (2022). Adsorption of metformin on activated carbon produced from the water hyacinth biowaste using H_3PO_4 as a chemical activator. *Sustainability,* 14(18): 11144.
47. Jimoh, O. S., Omotayo, I. A., and and Bello, O. S. (2023). Metformin adsorption onto activated carbon prepared by acid activation and carbonization of orange peel. *International Journal of Phytoremediation,* 25(2): 125-136.
48. Quesada, H. B., de Araújo, T. P., Cusioli, L. F., de Barros, M. A. S. D., Gomes, R. G., and Bergamasco, R. (2021). Evaluation of novel activated carbons from chichá-do-cerrado (Sterculia striata St. Hil. et Naud) fruit shells on metformin adsorption and treatment of a synthetic mixture. *Journal of Environmental Chemical Engineering,* 9(1): 104914.
49. Pap, S., Shearer, L., and Gibb, S. W. (2023). Effective removal of metformin from water using an iron-biochar composite: Mechanistic studies and performance optimisation. *Journal of Environmental Chemical Engineering,* 11(5): 110360.
50. Vareda, J. P. (2023). On validity, physical meaning, mechanism insights and regression of adsorption kinetic models. *Journal of Molecular Liquids,* 376: 121416.